Stability and physical properties of spherical excited scalar boson stars

Marco Brito,[1] Carlos Herdeiro,[1] Eugen Radu,[1] Nicolas Sanchis-Gual,[2,1] and Miguel Zilhão[1]

[1]*Departamento de Matemática da Universidade de Aveiro and Centre for Research and Development in Mathematics and Applications (CIDMA), Campus de Santiago, 3810-183 Aveiro, Portugal*

[2]*Departamento de Astronomía y Astrofísica, Universitat de València, Dr. Moliner 50, 46100, Burjassot (Valencia), Spain*

(Received 27 February 2023; accepted 14 March 2023; published 12 April 2023)

We study the time evolution of spherical, excited—with n radial nodes—scalar boson stars in general relativity minimally coupled to a complex massive scalar field with quartic self-interactions. We report that these stars, with up to $n = 10$, can be made dynamically stable, up to timescales of $t \sim \frac{10^4}{c\mu}$, where μ is the inverse Compton wavelength of the scalar particle, for sufficiently large values of the self-interactions coupling constant λ, which depends on n. We observe that the compactness of these solutions is rather insensitive to n, for large λ and fixed frequency. Generically, along the branches where stability was studied, these excited boson stars are not compact enough to allow for innermost stable circular orbits or light rings. Finally, we discuss the angular velocity of particles along timelike circular orbits, suggesting an application, for solutions in the Newtonian limit, to galactic rotation curves.

DOI: 10.1103/PhysRevD.107.084022

I. INTRODUCTION

Bosonic stars are localized self-gravitating lumps of bosonic fields, sustained by their own gravitational pull and (possibly) self-interactions, depending on the chosen model—see Refs. [1,2] for reviews. These hypothetical stars could be an alternative to (or coexisting with) black holes, e.g. [3–11]. Their dynamics can match real gravitational wave signals [12,13], and they have long been hypothesized as possible dark matter constituents [14–17]. In order for such stars to be realizable in the real world, however, they must be stable against small perturbations, which are unavoidable in any realistic astrophysical environment.

Let us consider spherically symmetric scalar boson stars, which will be the focus of this work—see e.g. [18–26] for different models. These stars may be found in different states, ranging from the fundamental or ground state ($n = 0$) to an infinitude of excited states ($n \geq 1$), analogous with the orbitals of the hydrogen atom—the $(n+1)$s orbital. The value of n is the number of nodes of the radial scalar profile. When a scalar field with no self-interactions is considered (i.e. mini-boson stars), excited states are possible, but they are unstable, decaying either to the fundamental state or collapsing into a black hole [27]. Mini-boson stars in the ground state, by contrast, are stable (along the appropriate branch) [28]. It was recently reported [29], however, that when a quartic self-interaction is introduced, it has a healing power which does stabilize $n = 1$ stars, for high enough values of λ, the coupling constant ruling the self-interactions. It may be expected that such healing behavior could extend to higher values of n. To assess and establish this possibility is a central purpose of this paper.

If excited stars are dynamically stable, they may have astrophysical applications. An interesting question is if such stars can be black hole foils, for instance, if they can be compact enough to allow the existence of special orbits that are characteristic of black holes, namely light rings [30] or an innermost stable circular orbit (ISCO) [31]. The lensing properties of ultracompact spherical bosonic stars (i.e. possessing light rings) has been considered in [32]. But recent evidence suggests such stars may be generically unstable [33,34]. On the other hand, even if they are not ultracompact, a certain structure of the timelike circular geodesics could void the central region of bosonic stars of emitting matter, therefore creating an "effective" shadow [9,10]. We will investigate if this can occur for the excited models we consider here. We remark that even if none of these features is present (ISCOs, light rings or the aforementioned special structure of timelike circular geodesics), boson stars could still mimic black hole data in certain situations, such as the emission of gravitational waves in particular events [12,13]. As another potential astrophysical application, we will consider the possibility that the excited boson stars could fit galactic rotation curves [14], and, consequently, whether they could be realistic models for dark matter galactic halos.

This paper is organized as follows. In Sec. II we describe the excited states of spherical boson stars, as solutions of the appropriate Einstein-Klein-Gordon system, discussing

their masses and compactness. In Sec. III we discuss the numerical relativity framework for our evolutions. In Sec. IV we discuss the main results both in the stability and formation scenarios. In Sec. V we study timelike geodesics around boson stars' spacetimes, probing if ISCOs or light rings are possible in any of our boson star models. We also study the structure of timelike circular orbits and a possible connection to galactic rotation curves. We close with a discussion and final remarks. For the rest of the article we shall use the metric signature $(-,+,+,+)$ and set $c = G = 1$.

II. THE MODEL

A. The action and field equations

We consider the following action describing Einstein's gravity minimally coupled to a complex, massive, self-interacting scalar field Φ (with complex conjugate Φ^*):

$$S = \int \left[\frac{R}{16\pi} - \frac{1}{2}(\Phi^*_{,\mu}\Phi^{,\mu} + U(|\Phi|^2))\right]\sqrt{-g}\mathrm{d}^4x, \quad (1)$$

which results in the following field equations:

$$R_{\mu\nu} - \frac{1}{2}g_{\mu\nu}R = 8\pi T_{\mu\nu}, \quad (2)$$

$$\Box\Phi = \frac{\mathrm{d}U}{\mathrm{d}|\Phi|^2}\Phi, \quad (3)$$

where

$$T_{\mu\nu} = \Phi^*_{,(\mu}\Phi_{,\nu)} - \frac{1}{2}g_{\mu\nu}[\Phi^*_{,\alpha}\Phi^{,\alpha} + U(|\Phi|^2)] \quad (4)$$

and

$$U(|\Phi|^2) = \mu^2|\Phi|^2 + \frac{\lambda}{2}|\Phi|^4, \quad (5)$$

where μ is the inverse reduced Compton wavelength of the quantum of the field and λ is the self-interaction coupling constant. We also define $\Lambda \coloneqq \lambda/(4\pi\mu^2)$. We choose units where $\mu = 1$, so that the only free parameter of the problem is Λ.

B. The ansatz

We are interested in spherically symmetric static configurations. These can be described by ansatz for the metric (in isotropic coordinates)

$$\mathrm{d}s^2 = -\mathrm{e}^{2F_0(r)}\mathrm{d}t^2 + \mathrm{e}^{2F_1(r)}[\mathrm{d}r^2 + r^2(\mathrm{d}\theta^2 + \sin^2\theta\mathrm{d}\varphi^2)] \quad (6)$$

and an ansatz for the scalar field

$$\Phi(x^\mu) = \phi(r)\mathrm{e}^{-\mathrm{i}\omega t}, \quad (7)$$

where $\omega > 0$ is the field's frequency. The time dependence is necessary to avoid Derrick-type obstructions (also known as virial theorems in this context [35]) to the existence of time independent stable scalar lumps [36]. Such dependence is canceled in the stress-energy tensor, since it only depends on the absolute value of the field and its gradients.

C. The boundary conditions

We have to solve the Einstein-Klein-Gordon equation system, composed by Eqs. (2) and (3). The system consists of second-order ordinary differential equations for the functions F_0, F_1 and ϕ along with two boundary conditions for each function. The boundary conditions at the origin to ensure regularity are given by

$$\partial_r F_{0,1}(0) = 0, \qquad \partial_r\phi(0) = 0,$$

whereas asymptotic flatness requires

$$F_{0,1}(r \to \infty) = \phi(r \to \infty) = 0.$$

D. Solutions

Solving the equations above will result in a set of infinite solutions with a different number of radial nodes n. The solutions will only exist for values of the frequency between $\omega_{\min} < \omega < \mu$. The solutions are located on curves such as the ones given in Fig. 1, which relate the Arnowitt-Deser-Misner (ADM) mass with the frequency of the stars.

In the ground state, solutions located between the maximum of the ADM mass and $\omega = \mu$ are stable. Analogously, for excited boson stars the corresponding region will be called the candidate stable branch, following [29], but in this case not every solution in this branch is stable. Although they have been found stable under infinitesimal perturbations that conserve the total mass and particle number [37], for generic perturbations they turn out to be unstable, both in the candidate stable and unstable branch [27]. As we will see, however, for large enough values of the self-interaction coupling constant they can be made stable.

These excited solutions, due to the existence of nodes, will be composed of a sphere of matter at the center, surrounded by n shells of matter. This can be seen in Fig. 2.

E. Mass and compactness

Knowing the mass of the obtained solutions is important to not only discuss the compactness of the stars, but also to study its evolution in time, because mass loss during the evolution signals a decay of the excited state, since states with lower n have less mass than their more excited counterparts [38], for the same frequency. As we are considering an asymptotically flat spacetime, with the vector $\vec{k} = \partial_t$ being timelike everywhere, the ADM mass

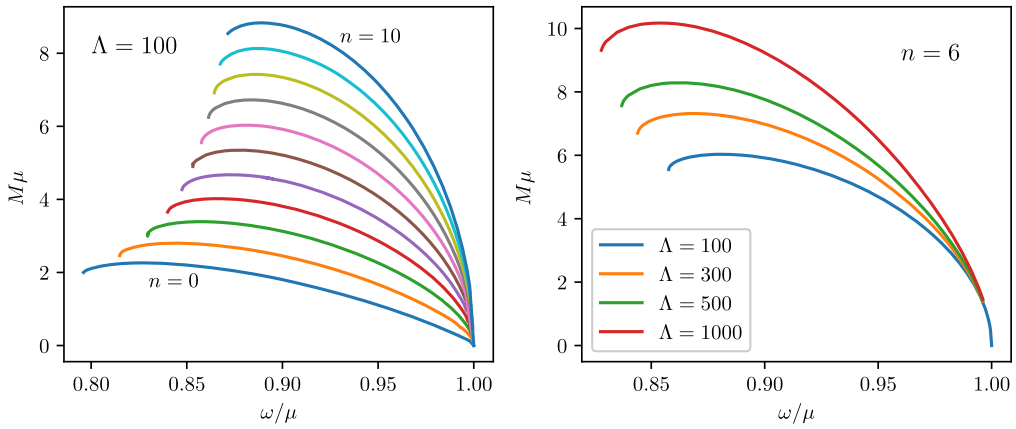

FIG. 1. ADM mass versus the frequency for boson star solutions with fixed Λ (left) and fixed n (right).

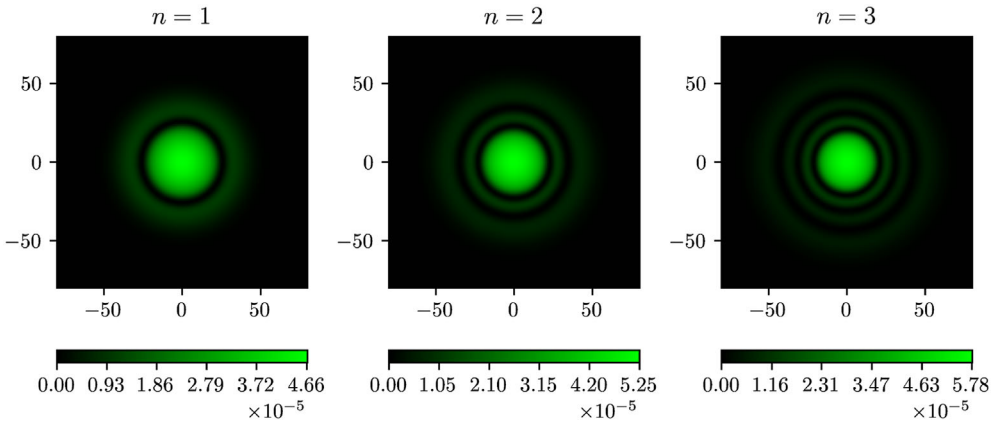

FIG. 2. Energy density of excited boson stars (omitting the θ coordinate) for $\Lambda = 500$, $\omega = 0.92$, where $R_{\text{areal}} = \sqrt{x^2 + y^2}$.

equals the Komar mass evaluated at infinity, and therefore we have

$$M_{\text{ADM}} = -\frac{1}{8\pi}\oint \nabla^{\alpha} k^{\beta} \mathrm{d}S_{\alpha\beta} = \int (T - 2T^{t}{}_{t})\sqrt{-g}\mathrm{d}r\mathrm{d}\theta\mathrm{d}\phi. \tag{8}$$

The mass of these stars increases with the value of Λ as $M \propto \sqrt{\Lambda}$ [18] and, for appropriate ranges of the scalar field mass and of the self-interactions coupling, it can be in the solar mass range, supermassive black holes range or dark matter halos range.

Furthermore we can define the compactness of an object as $C \coloneqq M/R$, where M is its mass and R its areal radius. There is a maximum compactness of $C = 0.5$ which corresponds to an object whose radius equals its own Schwarzschild radius, therefore becoming a black hole. Highly compact (but horizonless) stars could, in principle, permit the existence of light rings or ISCOs, if their areal radius is smaller than $3M$ or $6M$ respectively, at least in the case of an exterior Schwarzschild metric. The latter is only an approximation for spherical bosonic stars; indeed, scalar boson stars (for instance) are modeled by a scalar field which decays exponentially as $r \to \infty$, but only reaches zero at infinity. This means that unlike a fluid star where $T_{\mu\nu}$ vanishes for $r > r_{\text{surface}}$, there is no well-defined surface radius for boson stars. Still it is possible to define an effective radius for the star, beyond which we can neglect the remaining mass of the field, so that the spacetime beyond that radius is approximately a vacuum spacetime, i.e. $T_{\mu\nu} \simeq 0$. We shall define such an effective radius as the areal radius containing 99% of the ADM mass of the spacetime, denoted R_{99} [1,29]. Furthermore we define compactness of a boson star as

$$C \coloneqq \frac{M_{99}}{R_{99}}, \tag{9}$$

where $M_{99} \coloneqq 0.99 M_{\text{ADM}}$.

It is expected that the compactness can attain higher values with increasing Λ as the case for boson stars in the fundamental state [39], since the self-interaction is repulsive, and the mass increases with Λ. It should also increase

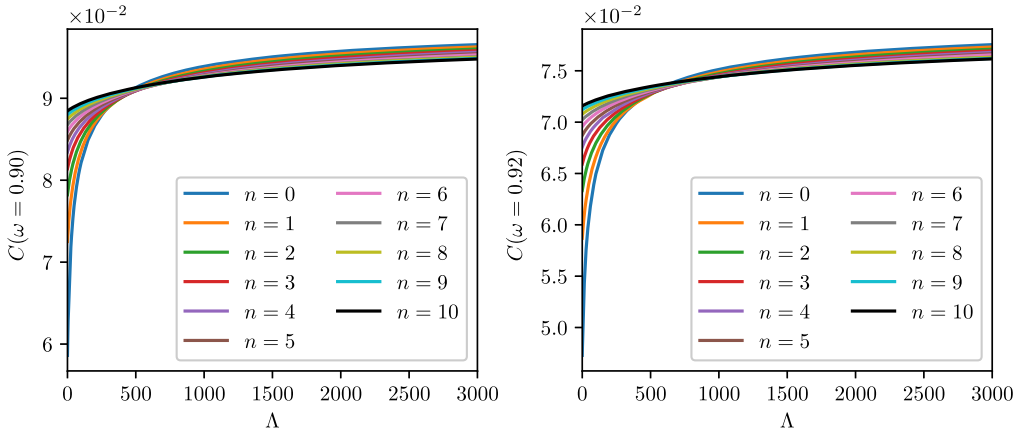

FIG. 3. Compactness as a function of Λ and n for $\omega = 0.90$ (left) and $\omega = 0.92$ (right).

as ω becomes smaller (within the candidate stable branch) since as $\omega \to 1$ we approach the Newtonian limit. One might thus expect that, for high enough values of Λ, the models may start exhibiting ISCOs and unstable circular orbit, as its compactness approaches that of a black hole. It turns out, however, that by increasing Λ, one seems to reach a limit of compactness [39], still well below that of black holes. Thus it is not possible to turn the star arbitrarily close to a black hole in this way. Our results reinforce this conclusion—Fig. 3—where one can see that the value of the compactness seems to asymptote to a value still far from the black hole value, for two fixed (illustrative) values of the frequency. One further notices that for Λ close to zero, stars with a larger n are more compact than stars with smaller n. But as $\Lambda \to \infty$ such behavior is reversed, and stars with smaller n are now more compact than stars with larger n.

As n increases there is a fairly common asymptotic value for the compactness. This is a trend observed in most quantities depending on n and Λ. The effective radius also increases with Λ and n as seen in Fig. 4, for boson stars

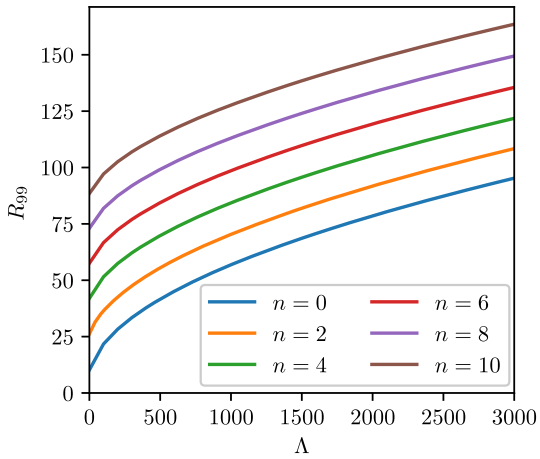

FIG. 4. Effective radius, R_{99}, as a function of Λ and n for $\omega = 0.90$.

with $\omega = 0.90$. As a consistency check, it was reported [39] that the maximum compactness in the stable branch for ground state solutions is $C_{\max} \approx 0.16$. Since the maximum value of the compactness is for $n = 0$, our results are in agreement with this limit, where $C_{\max} = 0.0965$. In order to reach this limit one would have to study stars with lower values of ω in the candidate stable branches. Moreover, for $n > 10$, we would not be able to go past this limit, since the trend for large Λ is that the compactness decreases as n increases.

III. NUMERICAL EVOLUTION

A. BSSN formalism and basic equations

Using a standard $3+1$ spacetime decomposition, a generic spacetime metric can be written in the form

$$ds^2 = g_{\mu\nu}dx^\mu dx^\nu = -\alpha^2 dt^2 + \gamma_{ij}(dx^i + \beta^i dt)(dx^j + \beta^j dt),$$

where α is the lapse function, β^i are the shift functions and γ_{ij} is the induced metric on the spatial hypersurfaces [40].

For the numerical evolutions the spatial metric is further written in the form

$$dl^2 = e^{4\chi}[a(t,r)dr^2 + r^2 b(t,r)d\Omega^2],$$

where $d\Omega^2 = d\theta^2 + \sin^2\theta d\varphi^2$ and $a(t,r)$ and $b(t,r)$ are two nonvanishing conformal metric functions, being related to the physical metric by the conformal decomposition $\gamma_{ij} = e^{4\chi}\hat{\gamma}_{ij}$ with $e^\chi = (\gamma/\hat{\gamma})^{1/12}$, where γ and $\hat{\gamma}$ are the determinant of the physical and conformal 3-metrics respectively. We shall use the Baumgarte-Shapiro-Shibata-Nakamura (BSSN) formulation [41,42] in spherical coordinates [43–45], which are suited for the problem at hand. The relevant differential equations for the problem are given in [29].

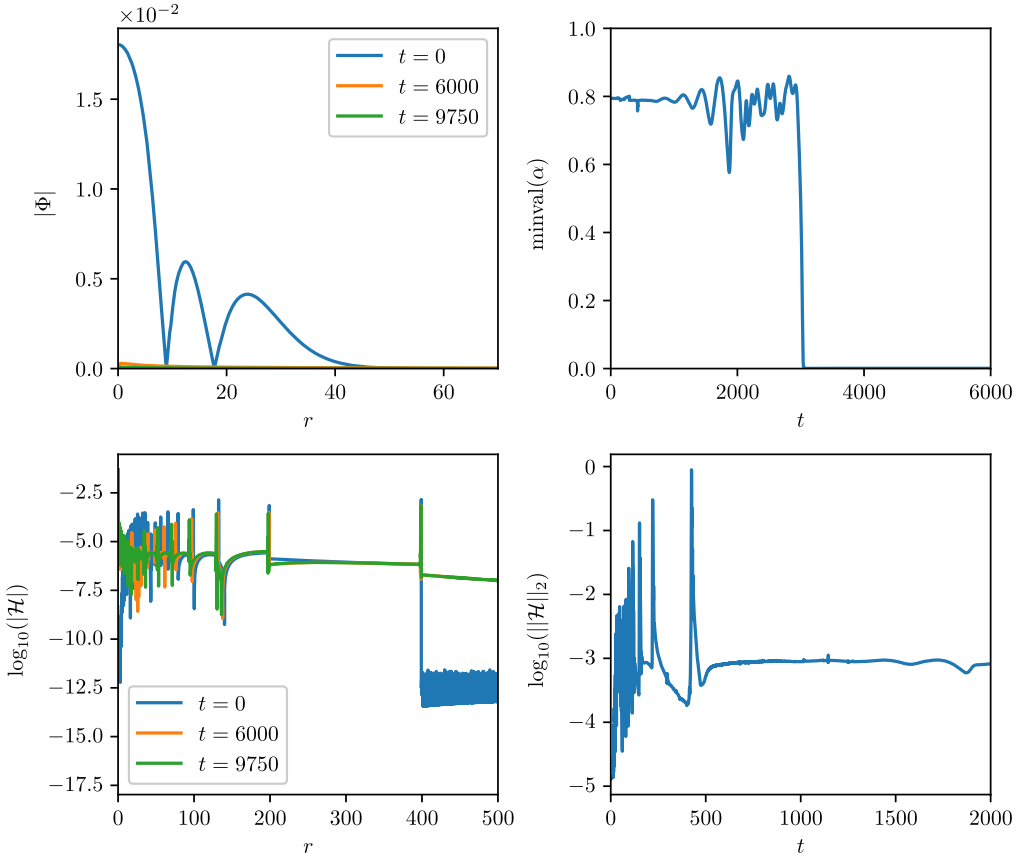

FIG. 5. Radial profile for different times (top left), minimum value of the lapse (top right), violation of the Hamiltonian constrain for certain times (bottom left) and the L2 norm of the Hamiltonian constraint ($||\mathcal{H}||_2$) (bottom right) for the boson star model $n = 2$, $\Lambda = 75$ and $\omega = 0.92$.

B. Numerical grid and stability

For the numerical evolutions we use the NADA code, a code for numerical relativity simulations in $1 + 1$D in spherical symmetry described in [44–50]. The BSSN and Klein-Gordon coupled equations are solved using a second-order partially implicity Runge-Kutta (PIRK) scheme [51,52]. The evolutions are performed in a logarithmic grid, with a maximum resolution of $\Delta r = 0.05$, a time step of $\Delta t = 0.3\Delta r$, the number of radial points being $n_r = 50000$ for stars with $n \leq 7$ and $n_r = 80000$ for the rest, and the outer boundary placed at $r_{\max} = 10000$. We impose radiative boundary (Sommerfeld) conditions at the outer boundary [44,53]. For the special case of $n = 2$, $\omega = 0.90$, $\Lambda = 125$ the number of radial points is $n_r = 100000$ and the outer boundary is placed at $r_{\max} = 20000$, since we extend the evolution to $t = 20000$ and we want to avoid reflections from the outer boundary. There are always some reflections, especially from the logarithmic grid when the resolution gets coarse.

We will not apply any specific perturbations to the stars, since the numerical truncation error suffices to break the staticity of the models, in case instabilities are present, triggering their time evolution. Moreover, since the stars are being evolved in a $1 + 1$D code in spherical coordinates under the assumption of spherical symmetry, the perturbations must be spherical. For nonspherical perturbations we need to evolve this model using a $3 + 1$D evolution code.

IV. DYNAMICAL EVOLUTION AND STABILITY

We now report the results of the evolution of the static configurations which are solutions to the Einstein-Klein-Gordon system up to a timescale[1] of $t \sim 10^4$ (where t is measured in units where $\mu = 1$). The evolutions were performed for $n = 0, 1, \ldots, 10$ for a variety of values of Λ in order to find stable boson stars. By stable boson stars we mean that within the considered timescale the initial and final radial profiles coincide, notwithstanding the existence of oscillations around an equilibrium point between the initial and final times.

[1]For stars whose composing bosons have the mass of the Higgs (125 GeV), the timescale is around 5×10^{-23} s, with a maximum mass around 10^{10} kg, much smaller than stellar masses. But for an ultralight boson with a mass of, say 10^{-10} eV, we have a timescale around 0.066 s with a maximum mass of $10M_\odot$.

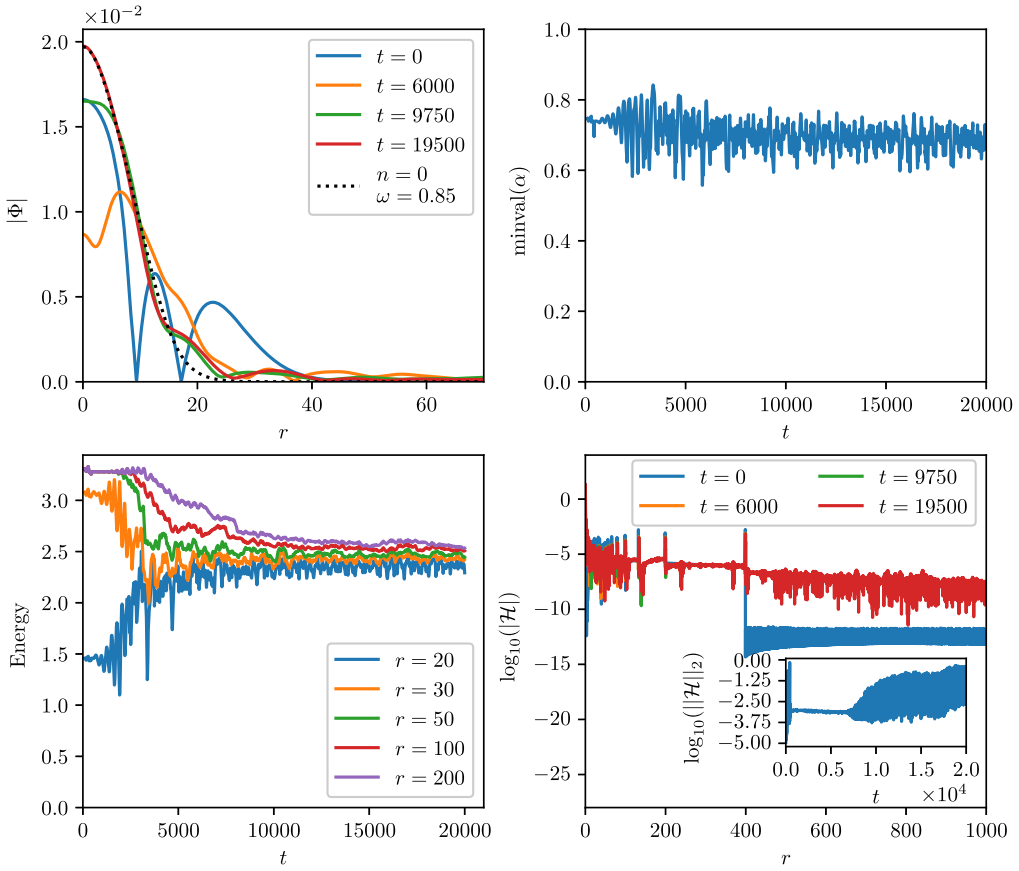

FIG. 6. Radial profile for different times and radial profile of candidate final state (top left), minimum value of the lapse (top right), the energy of the star at different spatial hypersurfaces (bottom left) and violations of the Hamiltonian constraint for certain times and the L2 norm of the Hamiltonian constraint (bottom right) for the boson star model $n = 2$, $\Lambda = 125$ and $\omega = 0.90$.

We have made a detailed study of solutions with $\omega = 0.90$, 0.92, and we shall present illustrative cases for one or the other frequency.[2] For the $n = 2$ case we shall present a more detailed study of the solutions, but such results are similar to the ones we have obtained for other $n > 2$.

A. $n = 2$ stars

1. Collapse into a black hole

For small values of Λ, the star cannot support itself against its own gravity, and thus it collapses into a black hole—see Fig. 5. This is supported by the fact that the minimum value of the lapse function α drops abruptly after a certain time ($t \approx 3000$ in this case), which typically means there was the formation of an apparent horizon.

2. Decay into a lower state

For intermediate values of Λ the stars are still unstable, but with a different outcome—see Fig. 6. The intermediate value of the self-interaction constant Λ is still unable to sustain the star, but it manages to prevent a complete gravitational collapse. It is clear that up to the end of the simulation, the star has not completely relaxed to the final state, as the minval(α) function shows, but we see in Fig. 6 (bottom left) that, since $r = 200$ can be considered as infinity (cf. Fig. 4), the star is losing mass/energy to infinity, which signals a decay. Furthermore this is accompanied by a redistribution of mass inside the star which is expected since during a decay the star will lose some of its shells, in this case seemingly losing all nodes. Since the star is not relaxed after $t = 10000$, we allowed the evolution to run for $t = 20000$. Even after $t = 20000$ the star is not completely relaxed; the plausible conclusion is that it decayed to the $n = 0$ state with a different frequency ($\omega = 0.85$), since the energy at $r = 200$ is around $E \approx 2.54$ which is the value of the ADM mass of the considered $n = 0$ star, which has an $M_{\mathrm{ADM}} \approx 2.44$. This suggests that the latter might be the end state of the evolution. Furthermore the central value of the scalar field is consistent with the one from a star with $n = 0$, $\Lambda = 125$, $\omega = 0.85$. For the rest of our models, we were not able to observe a decay of a boson star into a $n \neq 0$ state. We evolved several different unstable models that do not collapse into a black hole and found that they all ended

[2]These frequencies were chosen since for all values $n = 0, \ldots, 10$ they belong to the candidate stable branch. The smaller frequency approaches the maximum ADM mass, for $n = 10$.

up in the fundamental nodeless state. However, we have not explored the entire parameter space and therefore it seems likely that lower excited states can be formed from the decay of unstable excited boson stars.

Let us take this case to discuss the violations of the Hamiltonian constraint, which provide a diagnostic of the accuracy of our numerical evolution. Discussing it for this case is sufficient since it has the same features for all other cases, except when we have a collapse to a black hole, in which case the violation of the Hamiltonian constraint almost vanishes shortly after the initial instants. The radial profile of the Hamiltonian constraint in the region where the stars have support shows that the initial small violations decrease with time. However, the L2 norm of the Hamiltonian constraint in a larger radial region slowly increases as we get to the end of the evolution, $t = 10000$, but it remains small in the relevant region where the field is mostly located. It is worth noting that for all evolutions, the violation of the L2 norm of the Hamiltonian constraint at later times is larger for $\omega = 0.90$ than for $\omega = 0.92$, when it does not collapse into a black hole.

The spikes seen in the violation of the Hamiltonian constraint come from taking second derivatives of the variables interpolated from the initial data, which has a much lower number of points compared with the grid of the evolution code, especially at $r \geq 50$. This is further supported by the fact that after $r \approx 400$ we have no spikes since the last point of the initial data is around that value.

3. Threshold of stability for $n = 2$ stars

For high enough values of Λ we found that the stars become stable. We call such value of Λ the threshold of stability, since for $\Lambda > \Lambda_{\text{threshold}}$ the stars are always stable. We have found the threshold of stability for a star with $\omega = 0.90$ to be $\Lambda \simeq 160$ and for a star with $\omega = 0.92$ to be $\Lambda \simeq 150$. As seen in Fig. 7 on the leftmost picture, the star is fully relaxed. There is no mass loss since the star is stable. For the $n > 2$ boson stars studied, we also found a threshold of stability.

B. Stability of $n > 2$ stars

For the remaining cases of excited boson stars, with $n > 2$ we found a similar picture as for the $n = 2$ case, with distinct behaviors for low, intermediate and high values of Λ. Thus, we shall focus now on the thresholds of stability,

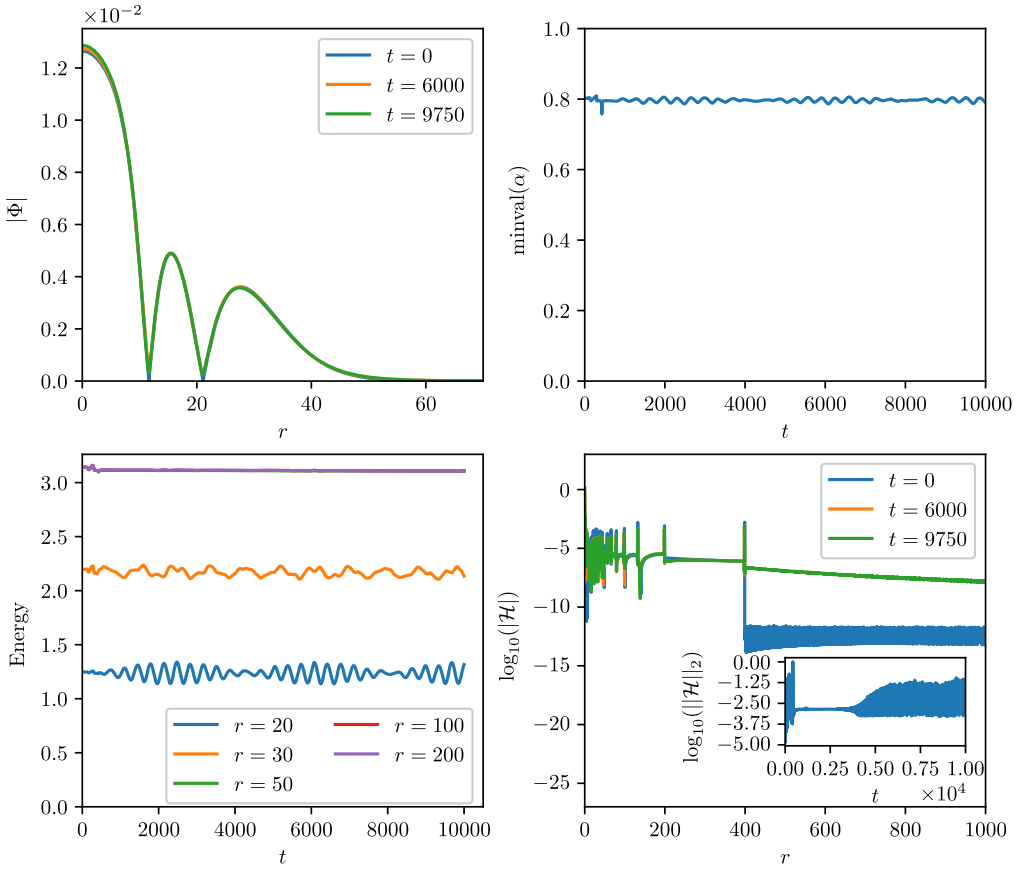

FIG. 7. Radial profile for different times (top left), minimum value of the lapse (top right), the energy of the star at different spatial hypersurfaces (bottom left) and violations of the Hamiltonian constraint for certain times and the L2 norm of the Hamiltonian constraint (bottom right) for the boson star model $n = 2$, $\Lambda = 150$ and $\omega = 0.92$.

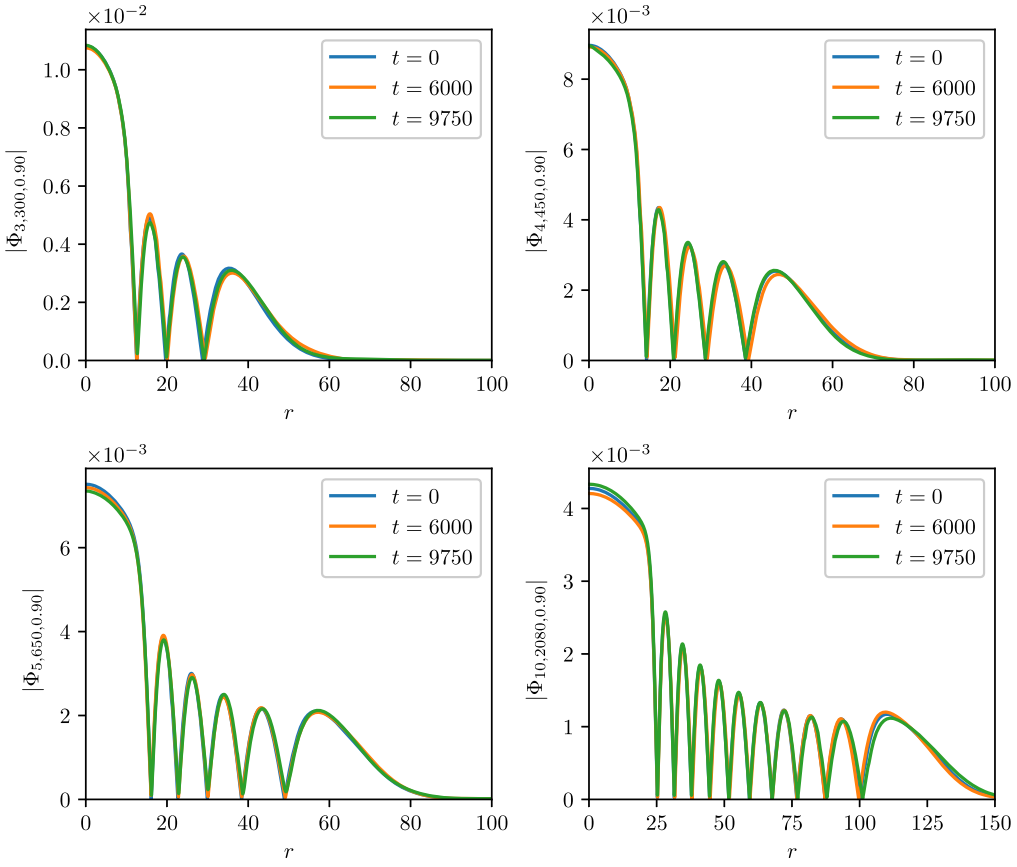

FIG. 8. Radial profiles $|\Phi_{n,\Lambda,\omega}|$ for the threshold of stability for several n.

that is, the values of Λ for which boson star models become stable. For $\Lambda < \Lambda_{\text{threshold}}$ the stars either collapse to black holes or into a lower state.

The results are quantitatively similar to the previous case, but now we have an n node star, and the threshold of stability happens for larger values of Λ. In Fig. 8 we have radial profiles for stable models of boson stars for illustrative values of n, and the threshold of stability is shown for two fixed frequencies, in terms of n in Table I. It is worth mentioning that for the $n = 0$ stars, we must evolve models with negative Λ, to find the threshold of stability, since they are already stable at $\Lambda = 0$. The potential $U(|\Phi|^2)$ in (5) becomes unbounded from below allowing for infinite negative energies. However, if we stick around the minimum of the potential we can avoid such problems, at least classically, where there is no quantum tunneling. But when Λ is negative enough, we cannot stick around the minimum and such models cannot even be evolved. For this case the thresholds of stability are $\Lambda = -4$ for $\omega = 0.90$ and, at the very least, $\Lambda = -6$ for $\omega = 0.92$, since for $\Lambda < -6$ the evolution crashes.

To conclude, we found that self-interactions can stabilize boson stars if Λ is greater than a certain threshold value. It is worth remarking that, as Λ grows, stars, initially collapsing to black holes, begin to avoid the collapse and eventually become stable when they reach $\Lambda_{\text{threshold}}$. We found that as n increases so does $\Lambda_{\text{threshold}}$, and it appears that they are related by a quadratic function as seen in Fig. 9. This suggests that for all values of n we can stabilize the stars as long as Λ is very large. It would be interesting to establish a mathematical proof of this statement.

TABLE I. $\Lambda_{\text{threshold}}$ for several boson star models. For $n = 0, 1$ the Λ of the last unstable model was taken to be $\Lambda_n - 1$. For $n > 1$ it was taken to be $\Lambda_n - 10$.

n	$\omega = 0.90$	$\omega = 0.92$
0	−4	−6
1	75	74
2	160	150
3	300	250
4	450	390
5	650	550
6	850	760
7	1160	1000
8	1380	1240
9	1750	1580
10	2080	1850

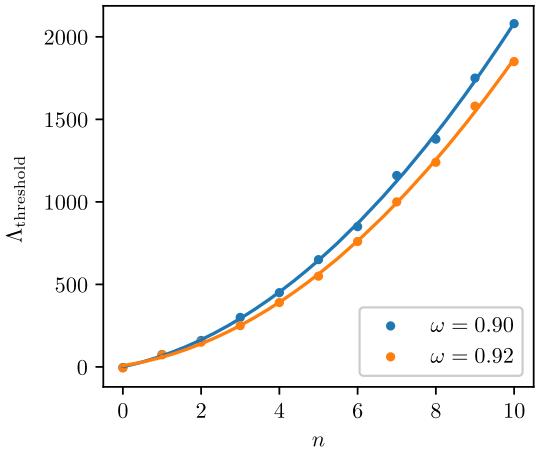

FIG. 9. The $\Lambda_{\text{threshold}}$ as a function of n.

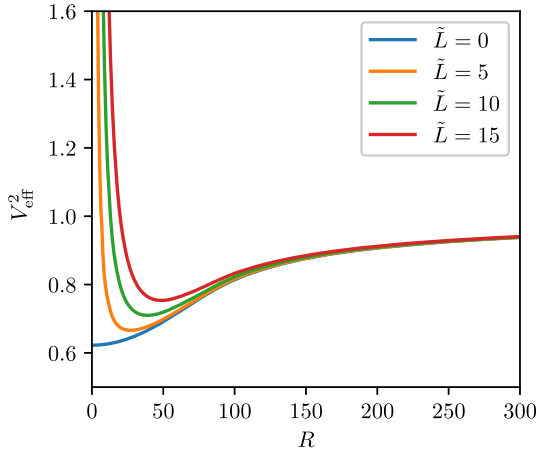

FIG. 10. Effective potential for $n = 0, \Lambda = 3000, \omega = 0.90$, the most compact star studied.

Adjusting a quadratic function to our points we obtain

$$\Lambda = 1.31 + 49.79n + 15.84n^2 \quad \text{for } \omega = 0.90, \quad R^2 = 0.9997,$$
$$\Lambda = 7.82 + 36.16n + 14.97n^2 \quad \text{for } \omega = 0.92, \quad R^2 = 0.9997,$$

where R^2 is the r-squared of the fit.

V. PHYSICAL FEATURES

A. Innermost stable circular orbit

Having established that sufficiently strong self-interactions can stabilize excited scalar boson stars, it becomes plausible, within the hypothesis that such scalar field models could exist, to consider the potential role of such stars in an astrophysical scenario. Then, they could have matter surrounding them. If they are compact enough, tidal disruptions might affect nearby objects leading to the appearance of an accretion disk, just like in some black holes and neutron stars. It is thus interesting to see if the models presented here are compact enough so they support special timelike orbits, like null unstable circular orbits and the ISCO.

In order to find the special orbits for the boson stars, we consider the effective potential that a particle in a timelike path feels when orbiting a boson star. We will work with an areal radius, since it is more intuitive to compare with the well-known values for the ISCO and unstable orbits of the Schwarzschild black hole. The transformation is easily done knowing that $R_{\text{areal}} = r_{\text{iso}} e^{F_1(r_{\text{iso}})}$. From now on we denote the areal radial coordinate as R. Then our line element (6) becomes

$$ds^2 = -e^{2F_0(R)}dt^2 + (1 - RF_{1,R})^2 dR^2 + R^2 d\Omega^2. \quad (10)$$

The derivation of the effective potential is a standard textbook exercise—see e.g. [54]. Consider now a particle orbiting a boson star. Due to spherical symmetry the orbit can be taken to lie on the equatorial plane, and thus $\theta = \pi/2$ and $p_\theta = 0$ throughout the whole trajectory, where $\vec{p}$ is the particle's four-momentum. Also since we have ∂_t and ∂_φ as Killing vectors due to the static[3] spherical symmetry of the problem, we can identify $-p_0$ as the energy E and p_φ as the angular momentum L. From the normalization of the momentum

$$g_{\mu\nu} p^\mu p^\nu = -m^2, \quad (11)$$

where m is the mass of the particle, we obtain

$$\underbrace{e^{2F_0}(1 - RF_{1,R})^2}_{\text{Always positive}} \left(\frac{dR}{d\tau}\right)^2 + \underbrace{e^{2F_0}\left(\frac{\tilde{L}^2}{R^2} + 1\right)}_{V^2_{\text{eff}}(R;\tilde{L})} = \tilde{E}^2, \quad (12)$$

where $\tilde{E} = E/m$, $\tilde{L} = L/m$, τ is the affine parameter and $V^2_{\text{eff}}(R;\tilde{L})$ is the effective potential, plotted in Fig. 10.

The ISCO is found by searching the minimum radius such that

$$\left.\frac{dV^2_{\text{eff}}}{dR}\right|_{R_{\min}(\tilde{L})} = 0. \quad (13)$$

For our potential such operation must be done numerically. Since the ISCO is the last stable orbit, we must find out for which values of $\tilde{L}$, $R_{\min}$ is the smallest. Again we do

$$\left.\frac{dR_{\min}(\tilde{L})}{d\tilde{L}}\right|_{\tilde{L}_{\text{ISCO}}} = 0 \quad (14)$$

so that we find at which $\tilde{L}$ a particle will stay on the ISCO and then $R_{\min}(\tilde{L}_{\text{ISCO}}) =: R_{\text{ISCO}}$. There is no ISCO or

[3]Our boson stars are only static after they relax to the final state since during the evolution they are dynamical.

unstable circular orbits for the boson stars studied here since there are stable orbits all the way down to $R \to 0$. The effective potential of the star is qualitatively analogous to the Newtonian potential of an orbiting particle in the Kepler problem, exhibiting a potential barrier. We conclude that the stars are not compact enough to support an ISCO. In fact the compactness of our stars is around $C = R_{99}/M_{99} \sim 0.1$. In order to see an ISCO the effective radius must be at least below $6M$. Even in the case reported by [39], $C^{-1} = 6.25$, we still do not have an ISCO. A similar analysis, with adequate adaptations, shows these stars, within the branch studied, have no light rings.

B. Angular velocity of particles

In [9] (see also [10]) it was observed that if the structure of timelike circular orbits around a spherical boson star are such that the angular velocity along the orbits attains a maximum, for an orbit with a nonvanishing radius, then the magnetorotational instability (MRI)—a mechanism driving the loss of angular momentum, and therefore driving matter toward the center of the star—could cease to be efficient. Thus, such a feature could create a void of matter in the core of the star and an effective shadow, under particular observation conditions. It is thus interesting to examine if such a feature could exist for the models of excited boson stars we are considering.

The angular velocity of a particle, as measured by an observer at infinity, is given by $\mathrm{d}\varphi/\mathrm{d}t$ which is, for an equatorial orbit,

$$\Omega := \frac{\mathrm{d}\varphi}{\mathrm{d}t} = \frac{\mathrm{d}\varphi/\mathrm{d}\tau}{\mathrm{d}t/\mathrm{d}\tau} = \frac{L}{E}\frac{\mathrm{e}^{2F_0(R)}}{R^2}. \tag{15}$$

For circular orbits we know that $\tilde{E}^2 = V_{\mathrm{eff}}^2$ and that $\frac{\mathrm{d}}{\mathrm{d}R}V_{\mathrm{eff}}^2 = 0$, since $\dot{R}(\tau) = \ddot{R}(\tau) = 0$, $\forall\,\tau$. This allows us to obtain the energy and angular momentum for each circular orbit. In our case this results in

$$\tilde{E} = \mathrm{e}^{F_0}\left(\frac{-F_{0,R}}{F_{0,R} - 1/R} + 1\right)^{1/2}$$
$$\tilde{L} = \left(\frac{-F_{0,R}}{F_{0,R}/R^2 - 1/R^3}\right)^{1/2}$$

for circular orbits with radius R. Then as a function of the radius of the orbit we have

$$\Omega(R_{\mathrm{orbit}}) = \sqrt{\frac{\mathrm{e}^{F_0}}{R_{\mathrm{orbit}}}\frac{\mathrm{d}\mathrm{e}^{F_0}}{\mathrm{d}R}\bigg|_{R_{\mathrm{orbit}}}}. \tag{16}$$

We are interested in studying how the angular velocity changes with R to assess the appearance of a maximum in the angular velocity for a certain orbit which can give accretion disks an inner edge even without the presence of an ISCO

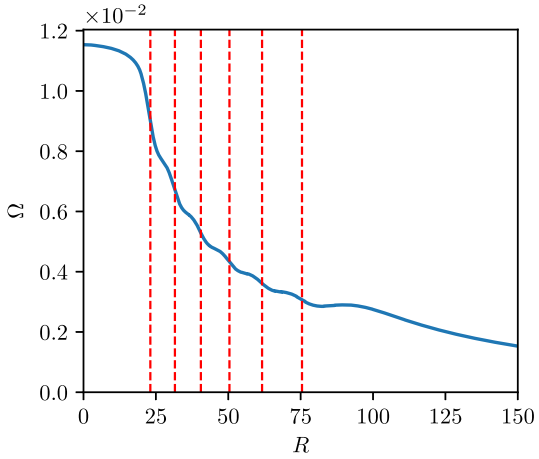

FIG. 11. Angular velocity as a function of R_{orbit} for $n = 6$, $\Lambda = 800$, $\omega = 0.92$. The vertical lines show the location of the nodes.

and resulting in an effective shadow for the compact object [9,10], due to the quenching of the MRI [55]. For mini-boson stars such features only show up for the unstable branch, having thus no relevance in an astrophysical scenario. For a free vector field instead of a scalar one, such features do show up [10] in the stable branch. Our excited boson stars, being composed of multiple spherical shells surrounding one another, and having a self-interaction, might behave differently from mini-boson stars.

The existence of nodes in our boson star models has an influence in the angular velocity of a particle, depending on whether its orbit is located around a node or not. In fact the existence of nodes causes the appearance of plateaus in the angular velocity, located in between the nodes of the radial function as seen in Fig. 11. As $R \to 0$, the angular velocity stops increasing, and a new plateau starts to appear. This holds even in the mini-boson star case, where the plateau is very small, being much more pronounced for large values of Λ. The reason is that as one approaches the origin, the matter contained inside a sphere of radius R also vanishes, and in a way that so does the variation of the orbital velocity.

In between the nodes we have a similar situation since, at the nodes we have a vacuum, which is followed by a shell of matter. Since part of the mass of the star is enclosed in a 2-sphere of $R < R_{\mathrm{node}}$, near the node the mass function is approximately constant which allows the particle to increase its angular velocity approximately[4] as $\sim\sqrt{M/R^3}$. But similarly to the $R \to 0$ case, as we cross the shell of mass between the nodes, the enclosed mass in a sphere of radius R will decrease, and $\Omega(R)$ will change as $\sim\sqrt{M(R)/R^3}$,

[4]This holds in a Newtonian approximation which does not take into account the pressure of the scalar field. This holds in a Newtonian approximation which does not take into account the pressure of the scalar field.

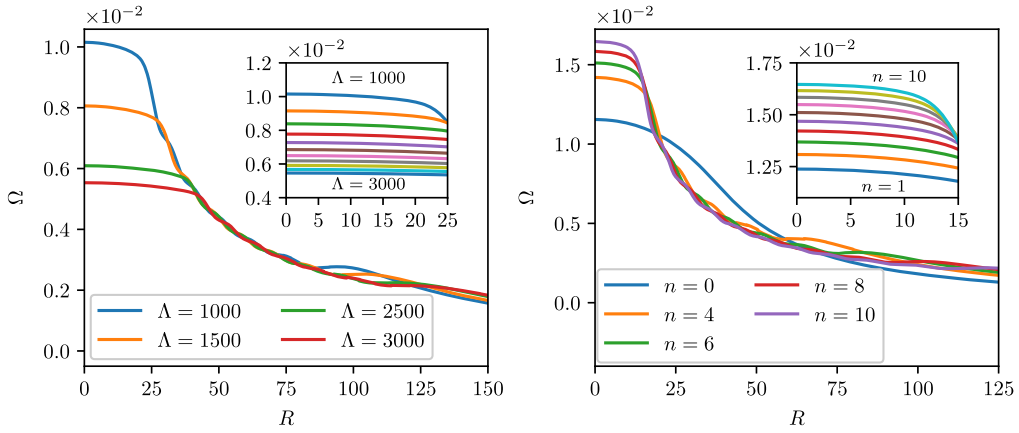

FIG. 12. Angular velocity as a function of $R_{\rm orbit}$ for $n = 6$, $\omega = 0.92$ for several Λ (left). Angular velocity as a function of $R_{\rm orbit}$ for $\Lambda = 300$, $\omega = 0.92$ for several n (right). Same qualitative behavior for $\omega = 0.90$.

which decreases the slope of the angular velocity curve. Also the radius of the star increases with Λ (although the mass also increases), which explains why the region of the plateaus is wider.

It is also worth noting that, as the value of Λ increases, the angular velocity near the center seems to approach an asymptotic value. The same also happens when Λ is fixed and n varies, again suggesting that for very large Λ the number of nodes seems not to matter. These features can be seen in Fig. 12.

Furthermore we report that for every $n \geq 3$ and for all Λ, for both of our studied frequencies, there is a maximum in the angular velocity, just before the angular velocity decays in a Keplerian fashion. That maximum is very small, questioning if it is a mere numerical artifact. However performing several tests, such as increasing the number of points, obtaining the solutions in other coordinate systems, and changing the interpolation, we were not able to get rid of this unexpected behavior. Assuming it is physical raises the question as to why it occurs and, moreover, only for $n > 2$, since no qualitative difference between $n = 2$ and $n = 3$ was to be expected.

C. Galactic rotation curves

The existence of nodes in boson stars has important consequences for the rotational velocity of matter around them. Facing these boson stars as dark matter suggests comparing these rotational velocities to galactic rotation curves.

As it is well known, the rotational velocity of stars in galaxies does not follow the expected Keplerian behavior $v_{\rm rot} \simeq \sqrt{GM(R)/R}$, the further we get from the center of the galaxy, where $M(R)$ is the mass of the visible or luminous matter enclosed in a sphere of radius R (for a review of dark matter in galaxies and its interaction with the baryonic matter see Ref. [56]). Since we have a high density of matter distributed around the center, at first $v_{\rm rot}$ increases, but once we are past that region, $v_{\rm rot}$ should decrease as $\propto \sqrt{1/R}$. Instead it has been famously found that the rotational velocity does not decrease in this way well past the region which contains the luminous matter. One proposed explanation is that galaxies are surrounded by dark matter halos, which could hypothetically be galactic scale boson stars.

The existence of plateaus in the $\Omega(R)$ plots hints at an increase of the rotational velocity in certain regions. The rotational velocity is defined as $v_{\rm rot} \coloneqq R\Omega$, and a plot versus the radius of orbit is given in Fig. 13. Excited boson stars with self-interactions had already been proposed as candidates to galaxy halos in [14]. This analysis is, however, different from ours, since therein the Newtonian rotational velocity is used, which does not take into account the pressure which is non-negligible [57].

We can divide the plots in Fig. 13 into three regions. First, near $R = 0$ there is a steep linear increase in $v_{\rm rot}$. This is expected since galaxies have a distribution of visible mass at the center which decreases as $R \to R_{\rm 1st\ node}$. This is also what is expected assuming a Keplerian $v_{\rm rot}$ for galaxies, since the observable mass is also mainly located at the center. However beyond the visible mass, $v_{\rm rot}$ should decay as $\sqrt{1/R}$, which is not the case, as experimental evidence shows that it increases linearly. Then there is a second region where the rotational velocity increases almost linearly albeit with some small oscillations, caused by the nodes. As the number of nodes increases the size of this region also increases, so stars with many nodes could explain the increase of rotational velocities in galaxies. In the last region we recover the expected $\sqrt{1/R}$ decay, which would correspond to a particle outside the galactic halo.

For a certain number of nodes, the increase of Λ only increases the effective radius of the star and thus the rotational velocity of the stars; although the qualitative features are the same for all Λ, they happen at a larger radius as Λ increases. The putative astrophysical

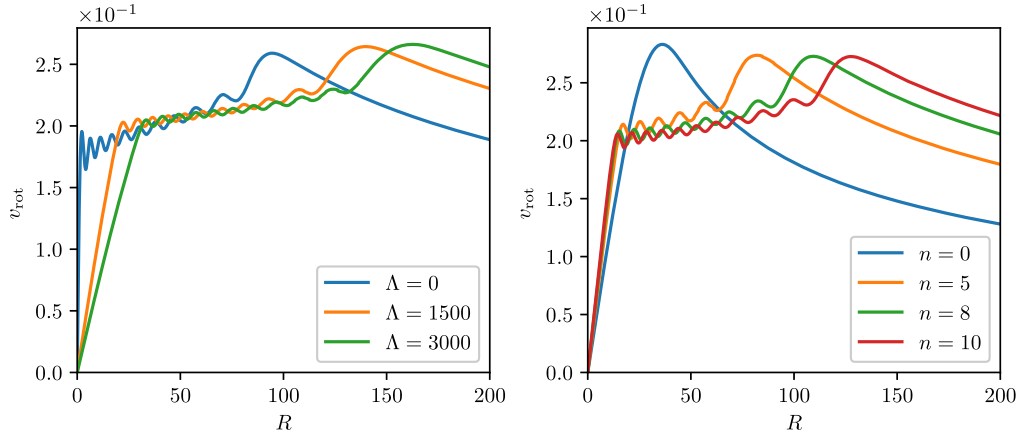

FIG. 13. Rotational velocity as a function of $R_{\rm orbit}$ for $n = 10$, $\omega = 0.92$ for several Λ (left). Angular velocity as a function of $R_{\rm orbit}$ for $\Lambda = 500$, $\omega = 0.92$ for several n (right). Same qualitative behavior for $\omega = 0.90$.

importance of Λ here is that a sufficiently large value can stabilize a boson star with a large number of nodes.

The foregoing discussion is, however, only a statement of principle. If we try to apply the studied models to real galaxies, the rotational velocity does not drop below $\sim 10^4$ km/s, whereas in realistic galaxies, velocities are $\sim 10^2$ km/s. The studied models are way too compact for applications to real galaxies and were studied within the context of stellar compact objects. If boson stars are to be the galactic dark matter halos, much more dilute boson stars, approaching the Newtonian limit, would be the correct framework.

VI. DISCUSSION AND CONCLUSION

It is well known that scalar boson stars in the ground state are stable against perturbations even in the absence of self-interactions, in some regions of the parameter space. In [29], however, it was shown that self-interactions can stabilize excited boson stars with one radial node, $n = 1$, for certain values of Λ. Using the same approach we have shown that such is also the case for stars with a number of nodes $2 \leq n \leq 10$, as long as Λ is greater than a certain threshold value. It is also expected that for sufficiently high enough values of Λ, stars with $n > 10$ should also be stable, since there is no reason for any qualitative difference between $n < 10$ and $n > 10$ stars. It would be interesting to attempt a mathematical proof of this statement. Furthermore, we have obtained an empirical quadratic relationship between $\Lambda_{\rm threshold}$ and n. We, however, leave the question of stability with respect to more general (nonspherical) perturbations for a future work, since it requires these models to be evolved in a $3 + 1$D code.

Although differing from mini-boson stars in many ways, these self-interacting excited boson stars are not compact enough so that features like ISCOs or light rings can be observed. We are focusing on candidate stable branch solutions, since only those can be made dynamically stable. It has been reported before that mini-boson stars can be highly compact in the unstable branch, which, however, has limited physical significance. The compactness was also found to be increasing with Λ, and it tends to an asymptotic value as $\Lambda \to \infty$, where stars with lower n are more compact than stars with larger n. But for large n the compactness of the stars seems to become (roughly) independent of n.

The angular velocity of test particles in circular orbits in boson stars' spacetimes was also studied, and it was found that the angular velocity as a function of r has several plateaus, that is, tends to become constant, near the location of the nodes. The existence of plateaus hints at peculiar angular velocity profiles, as found in Fig. 13, where there is a region far from the center where we witness an almost linear increase of the rotational velocity, which is qualitatively similar to what has been observed in galactic rotation curves. This suggesting fitting such models (after the threshold of stability) to real galactic rotation curves. No such comparison with data was made, since this required stars with a frequency ω close to 1, the Newtonian limit. Solutions with $\omega = 0.9999$ were obtained but even in that case the velocities were ten times larger than the velocities of realistic galaxies. One would need to obtain solutions in the Newtonian limit (solving the Schrödinger-Poisson equation), as done in [58] to fit with real galactic data, and then repeat the stability analysis. This is an interesting research direction for future work. We remark that it was previously discussed that stars with nodes could have a rotational velocity profile similar to those of galaxies; the potential stability of these objects, however, was not discussed. Our work shows that the stability issue could be solved within the paradigm of self-interactions.

Since these excited stars can, in principle, be realizable in an astrophysical context (even the dynamical formation of

such objects can be possible as discussed in [29] for $n = 1$ stars), one could also consider simulations of the collision of these objects, to assess their gravitational wave signals and compare them with real data from LIGO-Virgo-KAGRA detections.

ACKNOWLEDGMENTS

This work is supported by the Center for Research and Development in Mathematics and Applications (CIDMA) through the Portuguese Foundation for Science and Technology (FCT—Fundação para a Ciência e a Tecnologia), References No. UIDB/04106/2020 and No. UIDP/04106/2020. The authors acknowledge support from Projects No. CERN/FIS-PAR/0027/2019, No. PTDC/FIS-AST/3041/2020, No. CERN/FIS-PAR/0024/2021 and No. 2022.04560.PTDC. This work has further been supported by the European Union's Horizon 2020 research and innovation (RISE) Program No. H2020-MSCA-RISE-2017, Grant No. FunFiCO-777740 and by the European Horizon Europe staff exchange (SE) program HORIZON-MSCA-2021-SE-01 Grant No. NewFunFiCO-101086251. M. B. is supported by the FCT Grants No. GDG-2/2021/BI/CIDMA and No. 2022.09704.BD. This work is also supported by the Spanish Agencia Estatal de Investigación (Grant No. PID2021-125485NB-C21). N. S. G. is supported by the Spanish Ministerio de Universidades, through a María Zambrano Grant (No. ZA21-031) with Reference No. UP2021-044, funded within the European Union-Next Generation EU. Computations have been performed at the Argus and Blafis cluster at the U. Aveiro and at the Navigator Cluster at the LCA in U. Coimbra through Project No. 2021.09676.CPCA.

APPENDIX: NUMERICAL CONVERGENCE

In order to assess the quality of our numerical simulations we perform a convergence test, consisting of comparing different quantities from various grid resolutions and seeing if the results converge to the expected value. In order to perform our numerical evolutions we imported initial data into the code which was then interpolated to the evolution grid. We consider only numerical error coming from the finite difference operations, which dominates the error if we use resolutions coarser than the initial data resolution. In Fig. 14 we show the absolute value of the Hamiltonian constraint for four different resolutions at an instant of time $t = 1200$ for a stable boson star with $n = 2$, $\omega = 0.92$ and $\Lambda = 250$. We find the expected second-order convergence, since the PIRK time integrator is second order [44], for the first three resolutions ($\Delta r = 0.8$, $\Delta r = 0.4$, $\Delta r = 0.2$). However, as the resolution is further increased, the convergence order is reduced

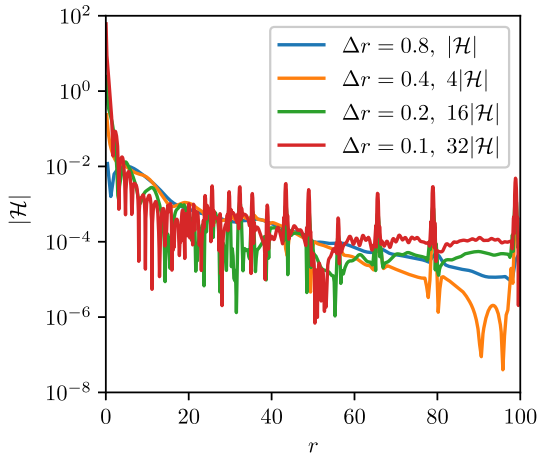

FIG. 14. Absolute value of the Hamiltonian constraint at $t = 1200$ for different resolutions for a boson star with $n = 2$, $\omega = 0.92$, $\Lambda = 250$.

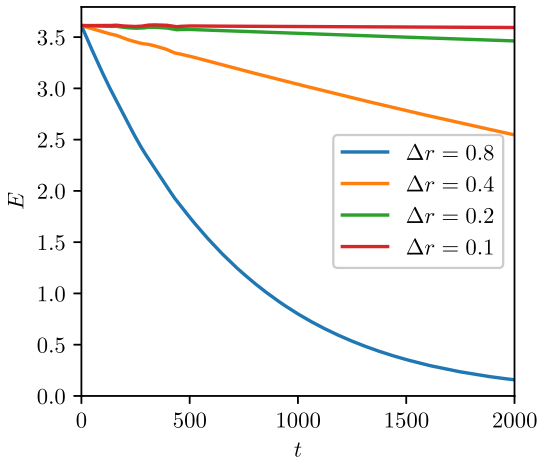

FIG. 15. Evolution of the total mass/energy for different resolutions.

to between first and second order. This is due to the fact that for high resolutions we are not improving anything compared with the initial grid.

We can also compare the drift of the evolution of the total mass as in Fig. 15. Since we consider a stable model the total mass should be constant throughout the evolution. However, due to numerical error, the mass decreases with time, and for low resolutions the numerical solutions are not good enough. Taking the deviation from the initial value of the mass $E(t = 0)$ we find that the order of convergence is 3, due to the fourth-order interpolatation, the second-order PIRK and the fourth-order finite differencing. The scaled functions can be seen in Fig. 16.

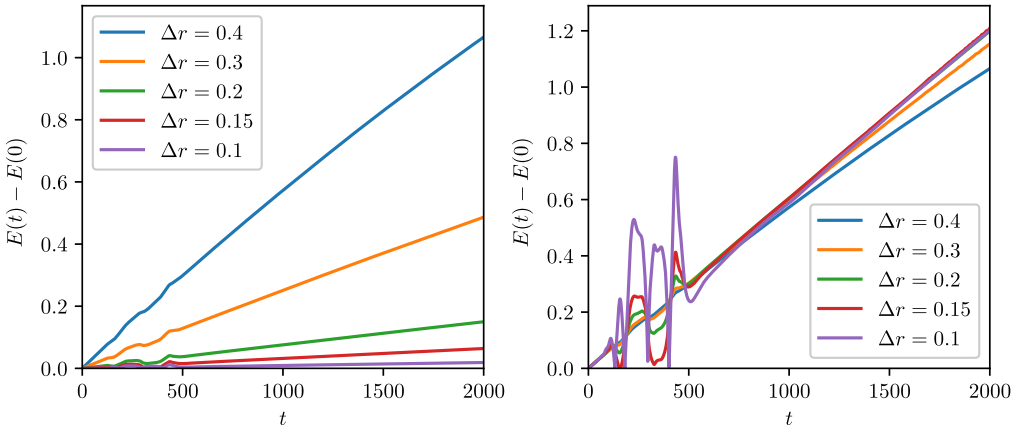

FIG. 16. Difference between total mass at $t = 1200$ and total initial mass (left) and rescaled functions to third-order convergence (right).

[1] F. E. Schunck and E. W. Mielke, Classical Quantum Gravity **20**, R301 (2003).
[2] S. L. Liebling and C. Palenzuela, Living Rev. Relativity **20**, 5 (2012).
[3] F. E. Schunck and A. R. Liddle, Lect. Notes Phys. **514**, 285 (1998).
[4] E. W. Mielke and F. E. Schunck, Nucl. Phys. **B564**, 185 (2000).
[5] E. Berti and V. Cardoso, Int. J. Mod. Phys. D **15**, 2209 (2006).
[6] F. S. Guzman and J. M. Rueda-Becerril, Phys. Rev. D **80**, 084023 (2009).
[7] F. H. Vincent, Z. Meliani, P. Grandclement, E. Gourgoulhon, and O. Straub, Classical Quantum Gravity **33**, 105015 (2015).
[8] M. Grould, Z. Meliani, F. H. Vincent, P. Grandclément, and E. Gourgoulhon, Classical Quantum Gravity **34**, 215007 (2017).
[9] H. Olivares, Z. Younsi, C. M. Fromm, M. De Laurentis, O. Porth, Y. Mizuno, H. Falcke, M. Kramer, and L. Rezzolla, Mon. Not. R. Astron. Soc. **497**, 521 (2020).
[10] C. A. R. Herdeiro, A. M. Pombo, E. Radu, P. V. P. Cunha, and N. Sanchis-Gual, J. Cosmol. Astropart. Phys. 04 (2021) 051.
[11] J. a. L. Rosa and D. Rubiera-Garcia, Phys. Rev. D **106**, 084004 (2022).
[12] J. C. Bustillo, N. Sanchis-Gual, A. Torres-Forné, J. A. Font, A. Vajpeyi, R. Smith, C. Herdeiro, E. Radu, and S. H. W. Leong, Phys. Rev. Lett. **126**, 081101 (2021).
[13] J. Calderon Bustillo, N. Sanchis-Gual, S. H. W. Leong, K. Chandra, A. Torres-Forne, J. A. Font, C. Herdeiro, E. Radu, I. C. F. Wong, and T. G. F. Li, arXiv:2206.02551.
[14] J. Lee and I. Koh, Phys. Rev. D **53**, 2236 (1996).
[15] A. Suárez, V. H. Robles, and T. Matos, Astrophys. Space Sci. Proc. **38**, 107 (2014).
[16] J. Eby, C. Kouvaris, N. G. Nielsen, and L. C. R. Wijewardhana, J. High Energy Phys. 02 (2016) 028.
[17] J. Chen, X. Du, E. W. Lentz, D. J. E. Marsh, and J. C. Niemeyer, Phys. Rev. D **104**, 083022 (2021).
[18] M. Colpi, S. L. Shapiro, and I. Wasserman, Phys. Rev. Lett. **57**, 2485 (1986).
[19] A. Bernal, J. Barranco, D. Alic, and C. Palenzuela, Phys. Rev. D **81**, 044031 (2010).
[20] B. Hartmann, J. Riedel, and R. Suciu, Phys. Lett. B **726**, 906 (2013).
[21] C. A. R. Herdeiro, A. M. Pombo, and E. Radu, Phys. Lett. B **773**, 654 (2017).
[22] M. Alcubierre, J. Barranco, A. Bernal, J. C. Degollado, A. Diez-Tejedor, M. Megevand, D. Nunez, and O. Sarbach, Classical Quantum Gravity **35**, 19LT01 (2018).
[23] Y. Brihaye and L. Ducobu, Phys. Lett. B **795**, 135 (2019).
[24] D. Guerra, C. F. B. Macedo, and P. Pani, J. Cosmol. Astropart. Phys. 09 (2019) 061; 06 (2020) E01.
[25] M. Bošković and E. Barausse, J. Cosmol. Astropart. Phys. 02 (2022) 032.
[26] A. Masó-Ferrando, N. Sanchis-Gual, J. A. Font, and G. J. Olmo, Classical Quantum Gravity **38**, 194003 (2021).
[27] J. Balakrishna, E. Seidel, and W.-M. Suen, Phys. Rev. D **58**, 104004 (1998).
[28] E. Seidel and W.-M. Suen, Phys. Rev. D **42**, 384 (1990).
[29] N. Sanchis-Gual, C. Herdeiro, and E. Radu, Classical Quantum Gravity **39**, 064001 (2022).
[30] P. V. P. Cunha and C. A. R. Herdeiro, Phys. Rev. Lett. **124**, 181101 (2020).
[31] J. F. M. Delgado, C. A. R. Herdeiro, and E. Radu, Phys. Rev. D **105**, 064026 (2022).
[32] P. V. P. Cunha, J. A. Font, C. Herdeiro, E. Radu, N. Sanchis-Gual, and M. Zilhão, Phys. Rev. D **96**, 104040 (2017).
[33] P. V. P. Cunha, E. Berti, and C. A. R. Herdeiro, Phys. Rev. Lett. **119**, 251102 (2017).
[34] P. V. P. Cunha, C. Herdeiro, E. Radu, and N. Sanchis-Gual, Phys. Rev. Lett. **130**, 061401 (2023).
[35] C. A. R. Herdeiro, J. a. M. S. Oliveira, A. M. Pombo, and E. Radu, Phys. Rev. D **106**, 024054 (2022).

[36] G. H. Derrick, J. Math. Phys. (N.Y.) **5**, 1252 (1964).
[37] P. Jetzer, Phys. Rep. **220**, 163 (1992).
[38] R. Friedberg, T. D. Lee, and Y. Pang, Phys. Rev. D **35**, 3640 (1987).
[39] P. Amaro-Seoane, J. Barranco, A. Bernal, and L. Rezzolla, J. Cosmol. Astropart. Phys. 11 (**2010**) 002.
[40] M. Alcubierre, *Introduction to 3+1 Numerical Relativity*, International Series of Monographs on Physics (Oxford University Press, Oxford, 2008).
[41] T. W. Baumgarte and S. L. Shapiro, Phys. Rev. D **59**, 024007 (1998).
[42] M. Shibata and T. Nakamura, Phys. Rev. D **52**, 5428 (1995).
[43] M. Alcubierre and M. D. Mendez, Gen. Relativ. Gravit. **43**, 2769 (2010).
[44] P. J. Montero and I. Cordero-Carrion, Phys. Rev. D **85**, 124037 (2012).
[45] N. Sanchis-Gual, J. C. Degollado, P. J. Montero, and J. A. Font, Phys. Rev. D **91**, 043005 (2015).
[46] N. Sanchis-Gual, J. C. Degollado, P. J. Montero, J. A. Font, and V. Mewes, Phys. Rev. D **92**, 083001 (2015).
[47] N. Sanchis-Gual, J. C. Degollado, P. J. Montero, J. A. Font, and C. Herdeiro, Phys. Rev. Lett. **116**, 141101 (2016).
[48] A. Escorihuela-Tomàs, N. Sanchis-Gual, J. C. Degollado, and J. A. Font, Phys. Rev. D **96**, 024015 (2017).
[49] F. Di Giovanni, S. Fakhry, N. Sanchis-Gual, J. C. Degollado, and J. A. Font, Phys. Rev. D **102**, 084063 (2020).
[50] F. Di Giovanni, S. Fakhry, N. Sanchis-Gual, J. C. Degollado, and J. A. Font, Classical Quantum Gravity **38**, 194001 (2021).
[51] I. Cordero-Carrión and P. Cerdá-Durán, arXiv:1211.5930.
[52] I. Cordero-Carrión and P. Cerdá-Durán, in *Advances in Differential Equations and Applications* (Springer, New York, 2014), pp. 267–278.
[53] M. Alcubierre, B. Bruegmann, P. Diener, M. Koppitz, D. Pollney, E. Seidel, and R. Takahashi, Phys. Rev. D **67**, 084023 (2003).
[54] C. W. Misner, K. S. Thorne, and J. A. Wheeler, *Gravitation* (Princeton University Press, Princeton, NJ, 2017).
[55] S. A. Balbus and J. F. Hawley, Astrophys. J. **376**, 214 (1991).
[56] P. Salucci, Astron. Astrophys. Rev. **27**, 2 (2019).
[57] F. E. Schunck, arXiv:astro-ph/9802258.
[58] S.-J. Sin, Phys. Rev. D **50**, 3650 (1994).